Supporting Information

Activation of a High-Valent Manganese-Oxo Complex by a Nonmetallic Lewis Acid

Regina A. Baglia, Maximilian Dürr, Ivana Ivanović-Burmazović, David P. Goldberg*

Department of Chemistry, The Johns Hopkins University, 3400 North Charles Street, Baltimore, Maryland 21218, United States
Department of Chemistry and Pharmacy, University of Erlangen-Nürnberg, 91058 Erlangen, Germany

Materials. The starting material $(TBP_8Cz)Mn^V(O)$ was synthesized according to published procedures.[1] The commercially available reagents $B(C_6F_5)_3$, $[(Me_2N)_3S]^+[Si(CH_3)_3(F)_2]^-$ (tris(dimethylamino)sulfonium difluorotrimethylsilicate, (TASF)), and dichloromethane (CHROMASOLV®) were obtained from Sigma-Aldrich at the best available purity and used as received. The compound 2,4-di-*tert*-butylphenol was purchased from Sigma-Aldrich and recrystallized from petroleum ether. The compound 2,4,6-tri-*tert*-butylphenol was purchased from Sigma-Aldrich and recrystallized from acetonitrile. Deuterated 2,4,6-tri-*tert*-butylphenol (2,4,6-TTBP-OD) was synthesized according to a published procedure.[2] Deuterated chloroform ($CDCl_3$, 0.05% v/v TMS) for NMR was purchased from Cambridge Isotopes.

Instrumentation. UV-vis spectroscopy was performed on a Hewlett-Packard 8452 diode-array spectrophotometer equipped with HPChemstation software. Gas chromatography was performed on an Agilent 6850 gas chromatograph fitted with a DB-5 5% phenylmethyl siloxane capillary column and equipped with a flame-ionization detector (FID). GC-FID response factors for 2,4-di-tert-butylphenol and 3,3',5,5'-tetra-tert-butyl-(1,1'-biphenyl)-2,2'-diol (bis(phenol) dimer) were prepared versus dodecane as the internal standard. ^{1}H-NMR spectra were recorded on a Bruker Avance 400 NMR instrument at 400 MHz. Electron paramagnetic resonance (EPR) spectra were recorded with a Bruker EMX spectrometer equipped with a Bruker ER 041 X G microwave bridge and a continuous-flow liquid helium cryostat (ESR900) coupled to an Oxford Instruments TC503 temperature controller. Spectra were obtained at 11 K under nonsaturating microwave power conditions (ν = 9.449 GHz, microwave power = 20.01 mW, modulation amplitude = 10 G, microwave frequency = 100 kHz, receiver gain = 5.02×10^3). EPR spectra were simulated by using the Bruker SimFonia Software version 1.26, 1997. Cryospray ionization mass spectrometry (CSIMS) measurements were recorded on a UHR-ToF Bruker

Daltonik (Bremen, Germany) maXis, an ESI-ToF MS capable of resolution of at least 40.000 FWHM, which was coupled to a Bruker cryospray unit. Detection was in positive-ion mode and the source voltage was held at 4 kV. The flow rates were 250 μL h^{-1}. The drying gas (N_2) was held at -45 °C and the spray gas was held at -50 °C. In source collision induced decomposition (ISCID) was achieved by increasing the DC potential between funnel 1 and funnel 2 in the double stage ion funnel transfer zone which leads to decomposition of dimeric ion moieties formed during the ionization process. The ISCID energy was held at 100 eV. The machine was calibrated prior to every experiment via direct infusion of the Agilent ESI-ToF low concentration tuning mixture, which provided an *m/z* range of singly charged peaks up to 2700 Da in both ion modes.

UV-vis spectral titrations for $Mn^{V}(O)(TBP_8Cz)$ + $B(C_6F_5)_3$. To a solution of $Mn^{V}(O)(TBP_8Cz)$ (5 μM) in CH_2Cl_2 (6 mL) was added 0.1 - 3.0 equiv of $B(C_6F_5)_3$ in 0.1 equiv increments from a stock solution in CH_2Cl_2. A color change of green to brown occurred, and a UV-vis spectrum was taken after each addition of Lewis acid, showing isosbestic conversion of green $Mn^{V}(O)(TBP_8Cz)$ (419, 634 nm) to brown $Mn^{IV}(O)(TBP_8Cz^{\bullet+})$:$B(C_6F_5)_3$ (419, 789 nm). The reaction mixture was allowed to equilibrate fully until no further spectral change was observed prior to the next addition of Lewis acid. A plot of the change in absorbance at 789 nm versus [$B(C_6F_5)_3$] resulted in the binding curve shown in Figure S1. This curve could be well fit by a 1:1 binding model , eq 1 – 4:

$$Mn^{V}(O)(TBP_8Cz)+B(C_6F_5)_3 \rightleftharpoons Mn^{IV}(O)(TBP_8Cz^{\bullet+})\text{-}B(C_6F_5)_3 \quad (1)$$

$$K_a = \frac{[Mn^{IV}(O)(TBP_8Cz^{\bullet+})\text{-}B(C_6F_5)_3]}{[Mn^{V}(O)(TBP_8Cz)][B(C_6F_5)_3]} \quad (2)$$

$$\frac{(A-A_0)}{(\varepsilon_{Mn(O)B}-\varepsilon_{Mn(O)})} = [Mn^{IV}(O)(TBP_8Cz^{\bullet+})\text{-}B(C_6F_5)_3] \quad (3)$$

$$\left[\mathrm{Mn^{IV}(O)(TBP_8Cz^{\bullet+})\text{-}B(C_6F_5)_3}\right] =$$

$$\frac{1}{2}\left[\left\{\left[\mathrm{B(C_6F_5)_3}\right] + \left[\mathrm{Mn^{V}(O)}\right]_i + \left(\frac{1}{K_a}\right)\right\} - \right.$$

$$\left.\sqrt{\left(\left[\mathrm{B(C_6F_5)_3}\right] + \left[\mathrm{Mn^{V}(O)}\right]_i + \left(\frac{1}{K_a}\right)\right)^2 - 4\left[\mathrm{B(C_6F_5)_3}\right]\left[\mathrm{Mn^{V}(O)}\right]_i}\right] \qquad (4)$$

The best fit of the plot in Figure S1 gives K_a = 2.03 (±0.5) x 10^7 M^{-1}.

Reaction of $Mn^{IV}(O)(TBP_8Cz^{\bullet+})$:$B(C_6F_5)_3$ with TASF. An amount of $Mn^{V}(O)(TBP_8Cz)$ (15 μM) was combined with $B(C_6F_5)_3$ (1 equiv, 10 μL of a 4.56 mM stock solution) in CH_2Cl_2 (3 mL), and the reaction was followed by UV-vis, showing rapid (~20 s) isosbestic conversion of $Mn^{V}(O)(TBP_8Cz)$ to $Mn^{IV}(O)(TBP_8Cz^{\bullet+})$:$B(C_6F_5)_3$ (419, 789 nm). A stock solution of TASF (20.0 mM) in $CH_2Cl_2$was prepared. An amount of TASF (10 μL, 4.4 equiv) was then added to the reaction mixture, resulting in a rapid change as seen by UV-vis, to give a final spectrum with peaks at 421, 634 nm corresponding to the regeneration of $Mn^{V}(O)(TBP_8Cz)$ (~87%, based on ε = 1.99 × 10^4 M^{-1} cm^{-1} at 634 nm). There was also a relatively sharp peak observed at 677 nm, corresponding to $[Mn^{III}(TBP_8Cz)F]^-$ (Figure S2).

Oxidation of the phenol substrate 2,4-DTBP. Product analysis. An amount of $Mn^{V}(O)(TBP_8Cz)$ (7.0 x 10^{-7} mol) was combined with $B(C_6F_5)_3$ (1 equiv) in CH_2Cl_2 (50 mL), and the reaction mixture was monitored by UV-vis until complete formation of $Mn^{IV}(O)(TBP_8Cz^{\bullet+})$:$B(C_6F_5)_3$ was observed. The phenol substrate 2,4-DTBP was then added in CH_2Cl_2 (250 μL of a 14.6 mM stock solution, 3.65 x 10^{-6} mol), and the spectrum for $Mn^{IV}(O)(TBP_8Cz^{\bullet+})$:$B(C_6F_5)_3$ (420, 789 nm) converted to the spectrum for $Mn^{IV}(OH)(TBP_8Cz)$ (λ = 443, 727 nm). The reaction mixture was concentrated under vacuum to ca. 500 μL, and dodecane was added as an internal standard. The solution was then immediately injected onto the

GC-FID for product analysis. The coupled product 3,3',5,5'-tetra-tert-butyl-(1,1'-biphenyl)-2,2'-diol was identified by comparison of retention time with an authentic sample, and quantitation was performed by integration of the peak and comparison with a calibration curve constructed with the internal standard. A yield of 77% (average of three runs) for the bis(phenol) product was obtained. Remaining 2,4-DTBP was also identified and quantified by GC-FID, giving 2.3 x 10^{-6} mol of unreacted phenol (3.3 equiv).

EPR spectroscopy for $Mn^{IV}(O)(TBP_8Cz^{\bullet+})$:$B(C_6F_5)_3$ + 2,4-DTBP. A concentrated solution of $Mn^{V}(O)(TBP_8Cz)$ (1.0 mM) was combined with $B(C_6F_5)_3$ (1 equiv) in CH_2Cl_2 (400 μL), and monitoring by UV-vis confirmed the formation of $Mn^{IV}(O)(TBP_8Cz^{\bullet+})$:$B(C_6F_5)_3$. Excess 2,4-DTBP (10 mg, 120 equiv) was added, and a change in the UV-vis spectrum was observed, resulting in a new spectrum for $Mn^{IV}(OH)(TBP_8Cz)$. The solution was then loaded into an EPR tube and slowly annealed at 77 K. EPR spectra were obtained at 12 K under non-saturating microwave power conditions (ν = 9.48 GHz, microwave power = 20.01 mW, modulation amplitude = 10 G, modulation frequency = 100 kHz). The resulting spectrum shows major features near g = 4 and g = 2 with hyperfine splitting from the ^{55}Mn nucleus (I = 5/2). The spectrum was satisfactorily simulated with a fictitious spin of S' = ½, and g = [4.61, 4.20, 1.92]; $A_{iso}(^{55}Mn)$ = [82, 86, 50] G. The 6-line signal observed at g = 2 is dominated by a relatively small amount of a Mn(II) impurity, which has been independently characterized from the decomposition of $Mn^{III}(TBP_8Cz)$ with HOTf and has a characteristic hyperfine coupling constant of $A_{iso}(^{55}Mn)$ = 120 G (Figure S6).

Kinetics of HAT with phenol substrates. A typical kinetic experiment was carried out by the following procedure. An amount of $Mn^{V}(O)(TBP_8Cz)$ (15 μM) was combined with $B(C_6F_5)_3$ (1 equiv, 25 μL of a 1.1 mM stock solution) in CH_2Cl_2 (2 mL), and the reaction was followed by

UV-vis. After complete formation of $Mn^{IV}(O)(TBP_8Cz^{\bullet+}):B(C_6F_5)_3$ was observed, a substituted phenol substrate (50 – 200 equiv) was added from a stock solution in CH_2Cl_2. The spectrum for $Mn^{IV}(O)(TBP_8Cz^{\bullet+}):B(C_6F_5)_3$ (420, 789 nm) decayed, and a new spectrum appeared for $Mn^{IV}(OH)(TBP_8Cz)$ (λ = 443, 727 nm). Plots of the growth in absorbance at 727 nm versus time appeared to be first-order up to 5 half-lives, and were well fit by the first-order expression shown in eq 5:

$$\boldsymbol{Abs_t = Abs_f + (Abs_0 - Abs_f)e^{-k_{obs}t}} \quad (5)$$

where Abs_t = absorbance at time t, Abs_f = final absorbance, Abs_0 = initial absorbance, and k_{obs} is the pseudo-first-order rate constant (Figure S9). A plot of k_{obs} versus concentration of phenol was found to be linear, and the slope of the best-fit line gave k_2, the second-order rate constant (Figure S9-S11).

Evans method measurement. To an amount of $Mn^{V}(O)(TBP_8Cz)$ (1 μmol) in $CDCl_3$ containing 0.05% TMS was added $B(C_6F_5)_3$ (1 equiv) as a stock solution in $CDCl_3$, to give a final concentration of 2.00 mM of Mn complex. A color change from green to brown was observed. The solution was placed in a NMR tube with a coaxial inner tube containing blank solvent ($CDCl_3$ with 0.05% v/v TMS). ^{1}H NMR spectra were recorded at 297.5 K, and the chemical shift of the TMS peak in the presence of the paramagnetic $Mn^{IV}(O)(TBP_8Cz^{\bullet+}):B(C_6F_5)_3$ complex was compared to that of the TMS peak in the inner tube containing only the TMS standard (Figure S7). The effective spin-only magnetic moment was calculated by a simplified Evans method analysis[3] according to Eq. 6:

$$\mu_{eff} = 0.0618\sqrt{\frac{\Delta\nu \mathrm{T}}{2\mathrm{fM}}} \quad (6)$$

where f is the oscillator frequency (MHz) of the superconducting spectrometer, T is the temperature (K), M is the molar concentration of the paramagnetic metal complex, and $\Delta\nu$ is the

difference in frequency (Hz) between the two reference (TMS) signals. In a control experiment, an Evans method measurement was performed on the $(TBP_8Cz)Mn^V(O)$ complex in the absence of $B(C_6F_5)_3$, and showed no shift in the standard TMS peak (Figure S8).

Cryospray Ionization Mass Spectrometry (CSIMS). All samples were prepared in a glovebox under Argon atmosphere by dissolving the given samples in dry CH_2Cl_2 and transferring them into a tandem cuvette for UV-vis experiments. One side was filled with $Mn^V(O)(TBP_8Cz)$ (1 mL of a 35.5 μM solution), and the other side was filled with $B(C_6F_5)_3$ (25 μL of an 1.4 mM stock solution) and complemented to 1 mL with dry CH_2Cl_2. UV-vis spectra were recorded before and after mixing. The reaction took place in about 15 seconds. MS measurements also were performed out of the solutions of the cuvette. Better results were obtained by preparing the solutions in the glovebox and direct transfer into Hamilton gastight syringes for direct infusion in the MS.

References:

(1) Lansky, D. E.; Mandimutsira, B.; Ramdhanie, B.; Clausén, M.; Penner-Hahn, J.; Zvyagin, S. A.; Telser, J.; Krzystek, J.; Zhan, R.; Ou, Z.; Kadish, K. M.; Zakharov, L.; Rheingold, A. L.; Goldberg, D. P. *Inorg. Chem.* **2005**, *44*, 4485.
(2) Zdilla, M. J.; Dexheimer, J. L.; Abu-Omar, M. M. *J. Am. Chem. Soc.* **2007**, *129*, 11505.
(3) Evans, D. F.; Jakubovic, D. A. *J. Chem. Soc., Dalton Trans.* **1988**, 2927.
(4) Reed, G. H.; Leigh, J. S.; Pearson, J. E. *J. Chem. Phys.* **1971**, *55*, 3311.

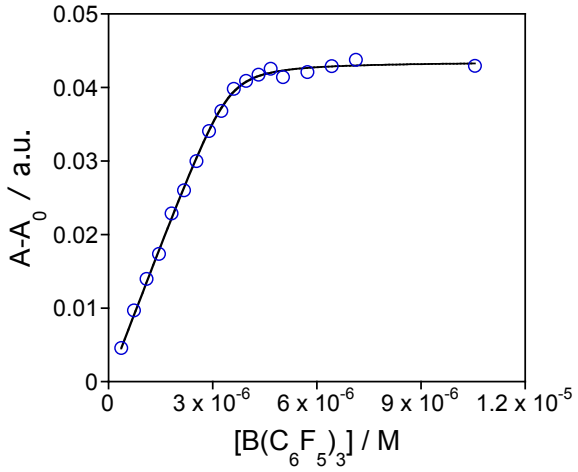

Figure S1. Binding isotherm at 789 nm resulting from the reaction of $Mn^{V}(O)(TBP_8Cz)$ (5 μM in 6 mL dichloromethane) and $B(C_6F_5)_3$.

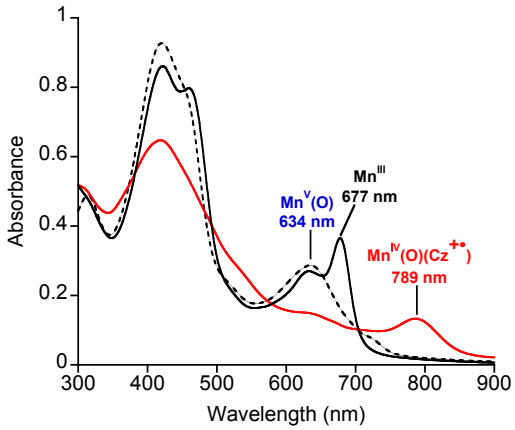

Figure S2. UV-vis spectral data for $Mn^{V}(O)(TBP_8Cz)$ (dotted line), $Mn^{IV}(O)(TBP_8Cz^{\bullet+}):B(C_6F_5)_3$ (red line), and after addition of TASF (4.4 equiv) (black solid line).

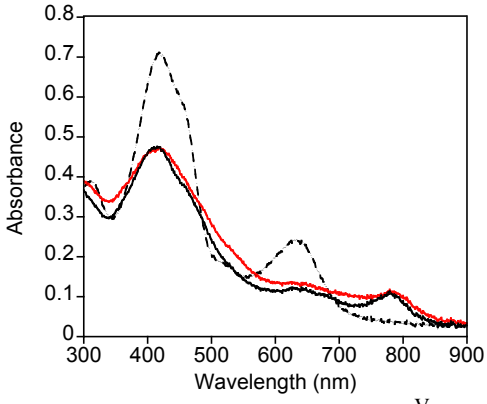

Figure S3. UV-vis spectral data for $Mn^{V}(O)(TBP_8Cz)$ (dotted line), $Mn^{IV}(O)(TBP_8Cz^{\bullet+}):B(C_6F_5)_3$ (red line), and after addition of tetrabutylammonium chloride (260 equiv) (black solid line).

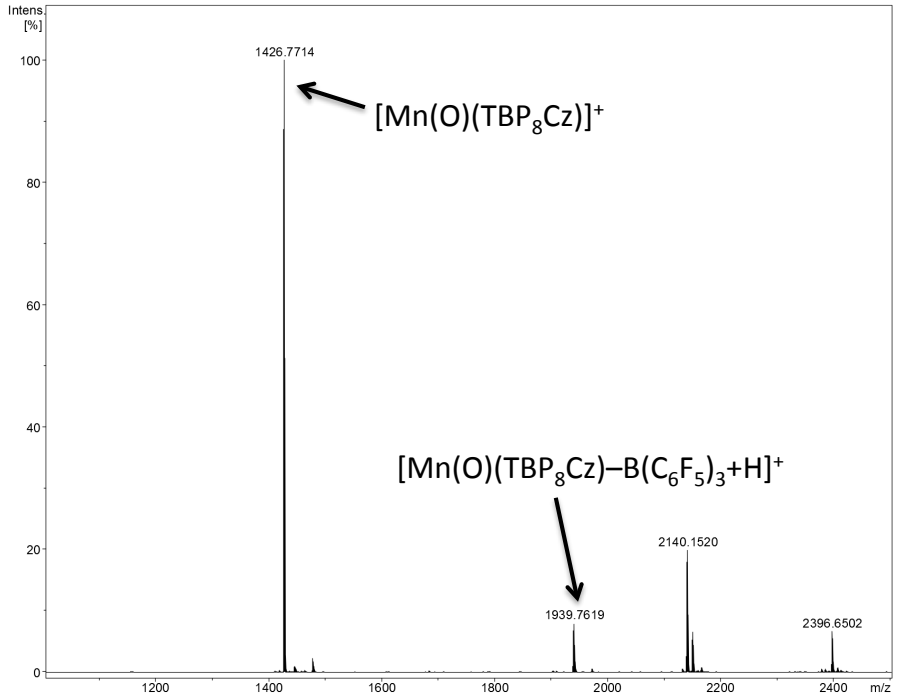

Figure S4. CSI-MS (positive mode, -50 °C) data from the reaction of $Mn^{V}(O)(TBP_8Cz)$ (35.5 μM in CH_2Cl_2) with $B(C_6F_5)_3$ (1 equiv).

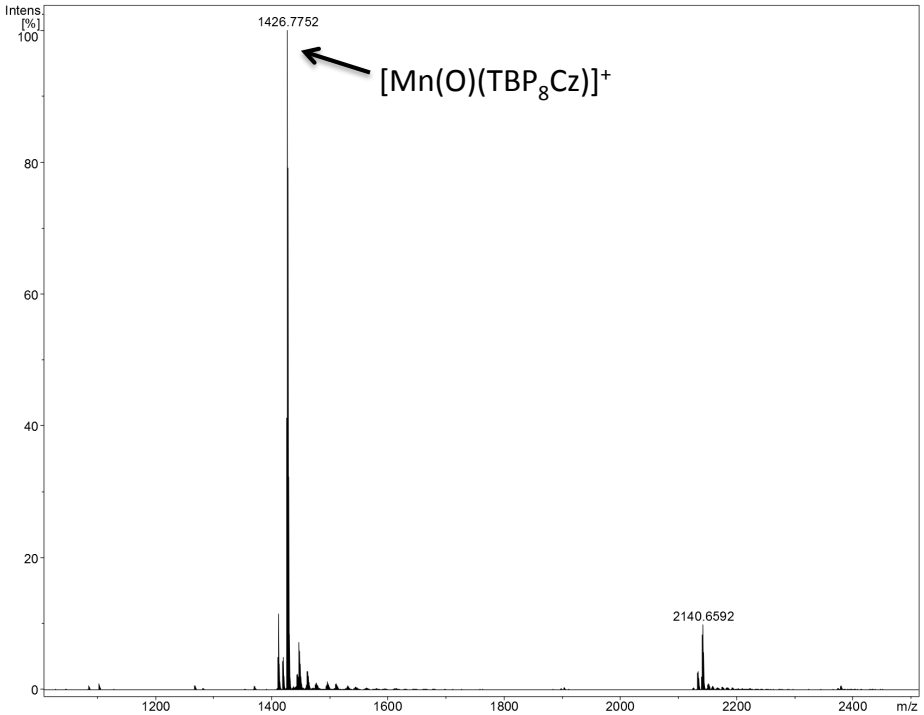

Figure S5. CSI-MS (positive mode, -50 °C) data for $Mn^{V}(O)(TBP_8Cz)$ (35.5 μM in CH_2Cl_2). Observed m/z 1426.7752; calculated m/z 1426.7710.

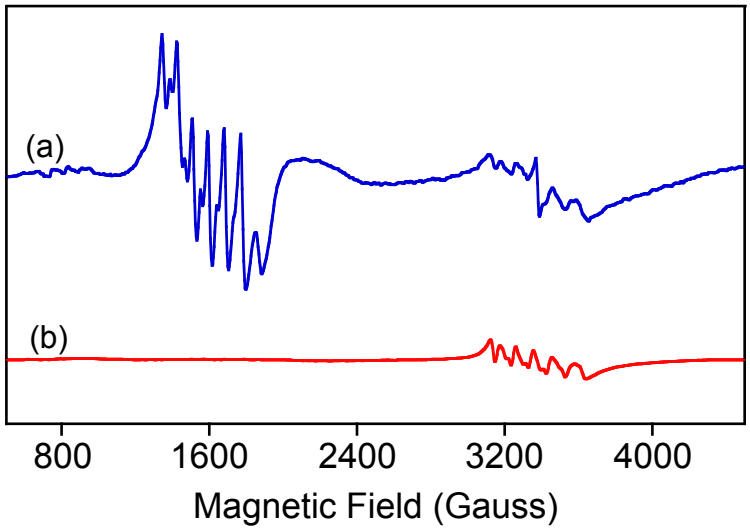

Figure S6. X-band EPR spectra at 12 K for (a) the reaction of $Mn^{IV}(O)(TBP_8Cz^{\bullet+}):B(C_6F_5)_3$ (1.0 mM) with 2,4-DTBP (120 equiv) (blue line) and (b) $Mn^{III}(TBP_8Cz)$ with excess HOTf in CH_2Cl_2 (red line). The 6-line pattern centered at g = 2 with $A_{iso}(^{55}Mn)$ = 120 G is a good match with other Mn^{II} complexes,[4] and corresponds to the major component seen at g = 2 in the blue spectrum.

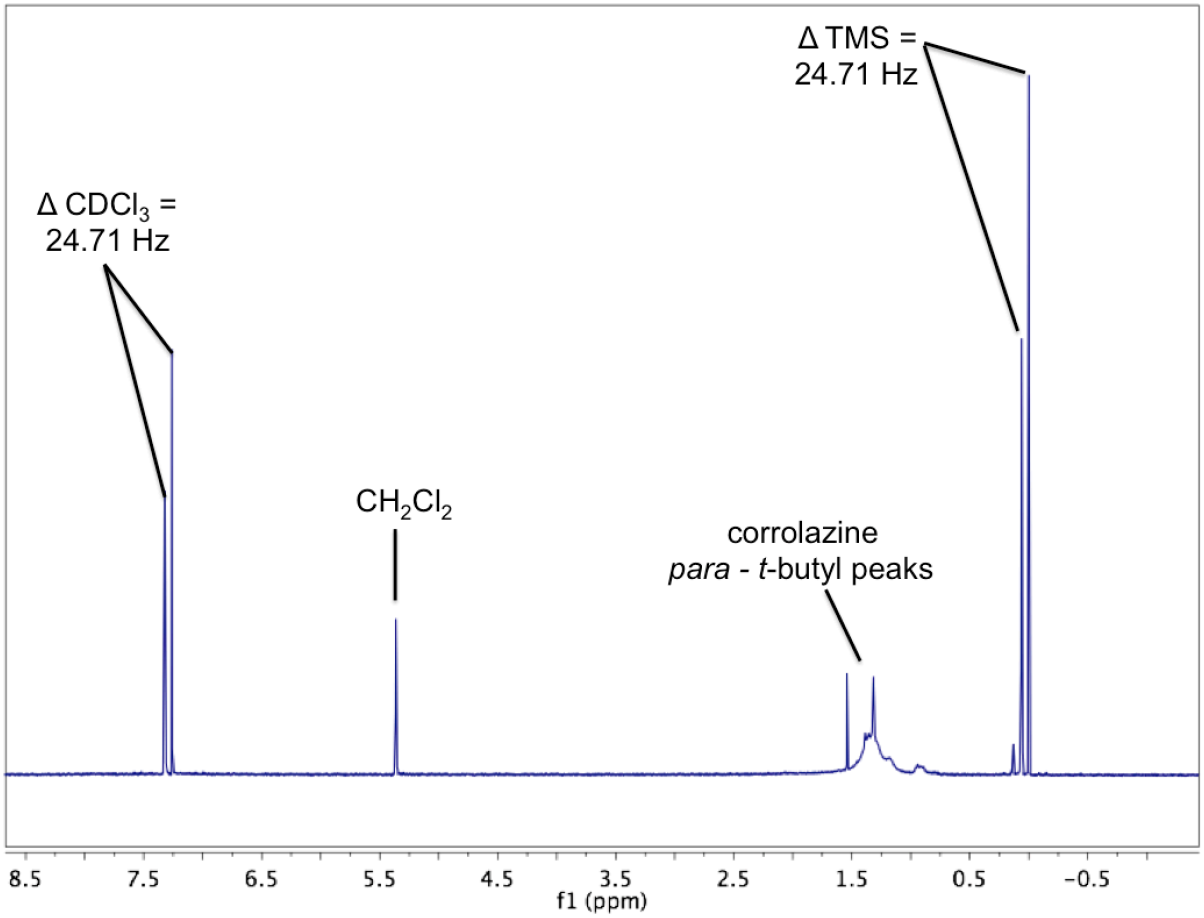

Figure S7. Evans method ^{1}H-NMR spectrum of $Mn^{IV}(O)(TBP_8Cz^{\bullet+}):B(C_6F_5)_3$ (2.00 mM) in $CDCl_3$ (0.05% TMS).

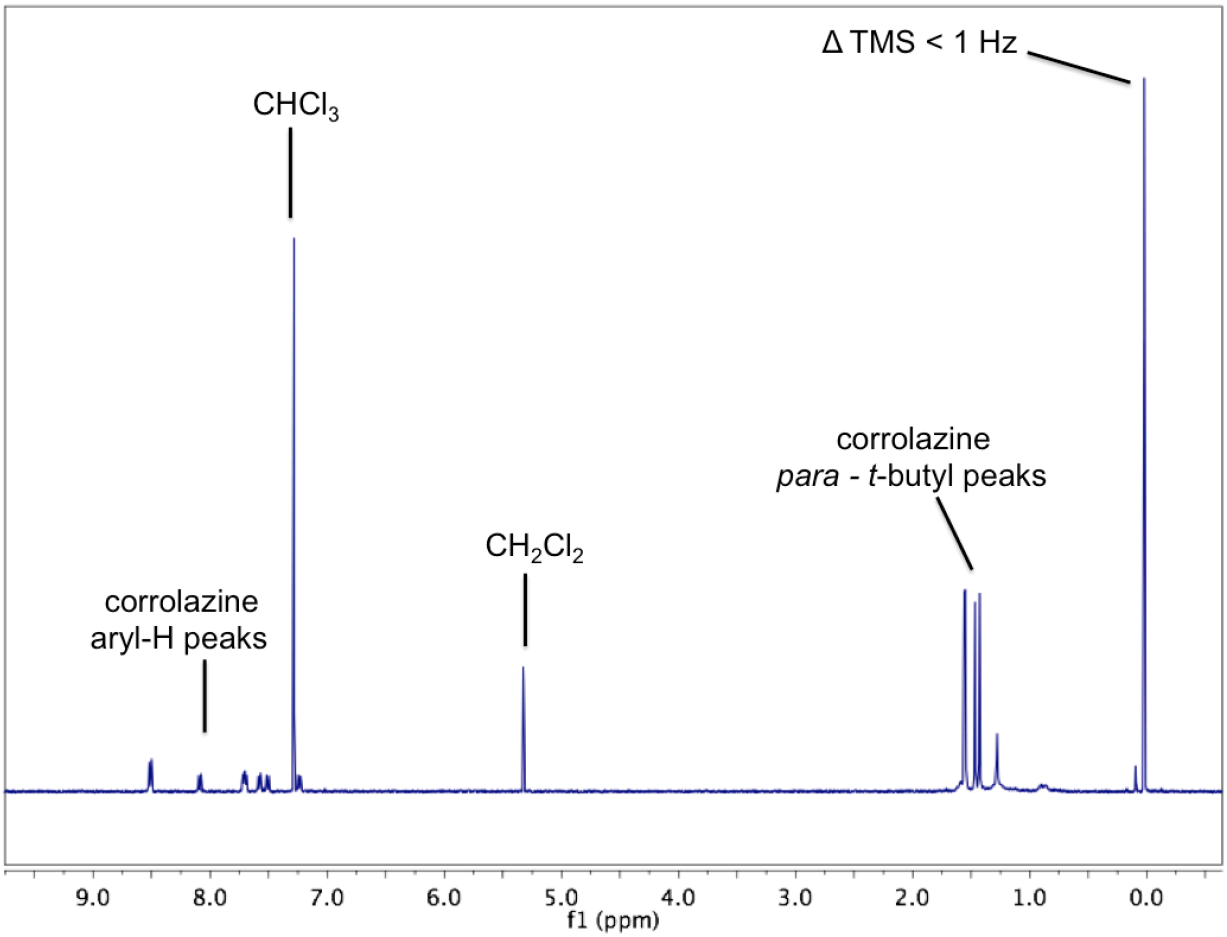

Figure S8. Evans method ^{1}H-NMR spectrum of $Mn^{V}(O)(TBP_8Cz)$ (2.00 mM) in $CDCl_3$ (0.05% TMS).

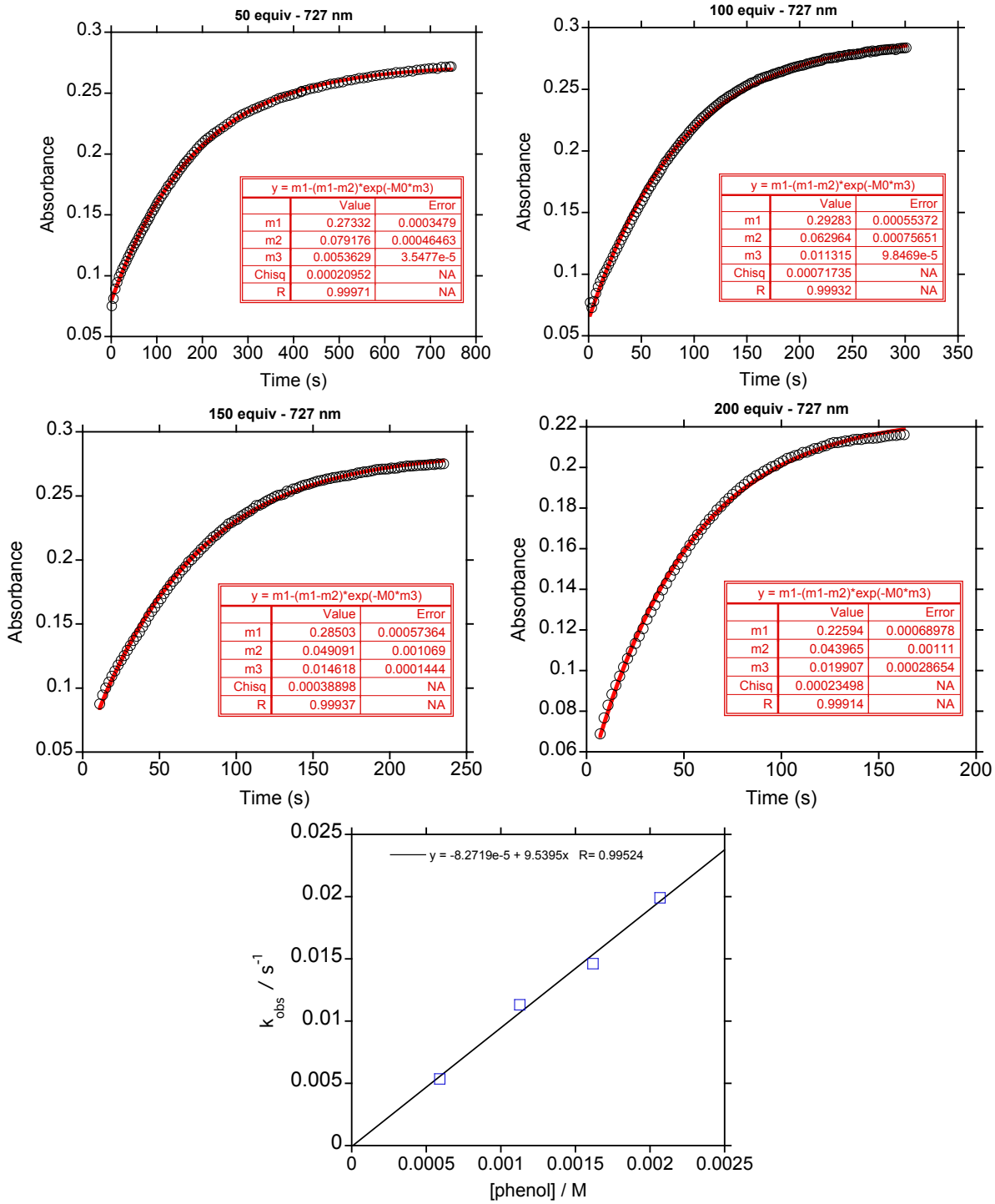

Figure S9. Kinetic plots of absorbance at 727 nm versus time for the reaction between $Mn^{IV}(O)(TBP_8Cz^{\bullet+})$:$B(C_6F_5)_3$ and 2,4,6-TTBP (50 – 200 equiv), and corresponding second order plot of k_{obs} versus [2,4,6-TTBP], where the slope of the best fit line gives $k_2 = 9.5 \pm 0.7$ M^{-1} s^{-1}.

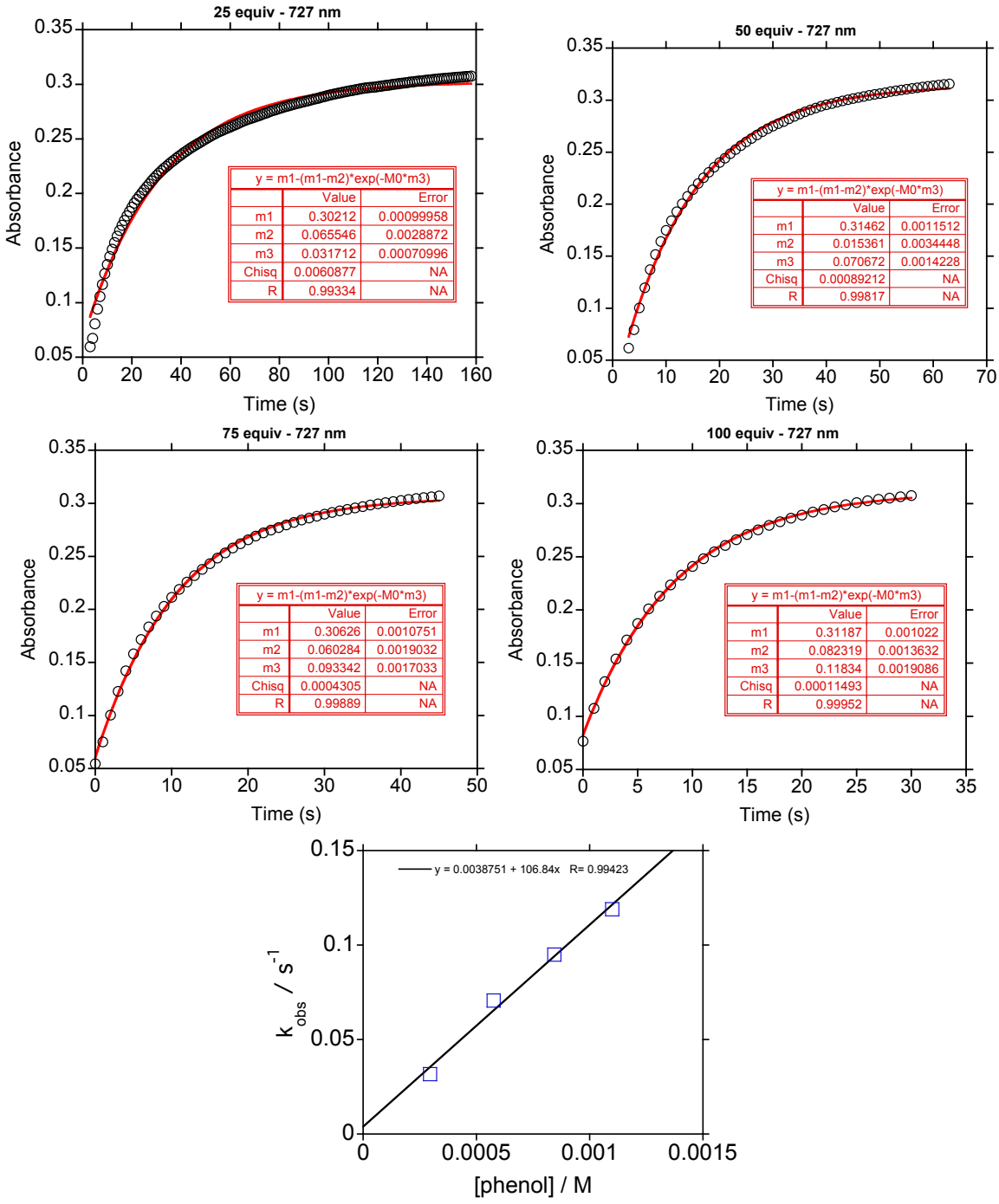

Figure S10. Kinetic plots of absorbance at 727 nm versus time for the reaction between $Mn^{IV}(O)(TBP_8Cz^{\bullet+})$:$B(C_6F_5)_3$ and 2,4-DTBP (25 – 100 equiv), and corresponding second order plot of k_{obs} versus [2,4-DTBP], where the slope of the best fit line gives $k_2 = 107 \pm 8$ M^{-1} s^{-1}.

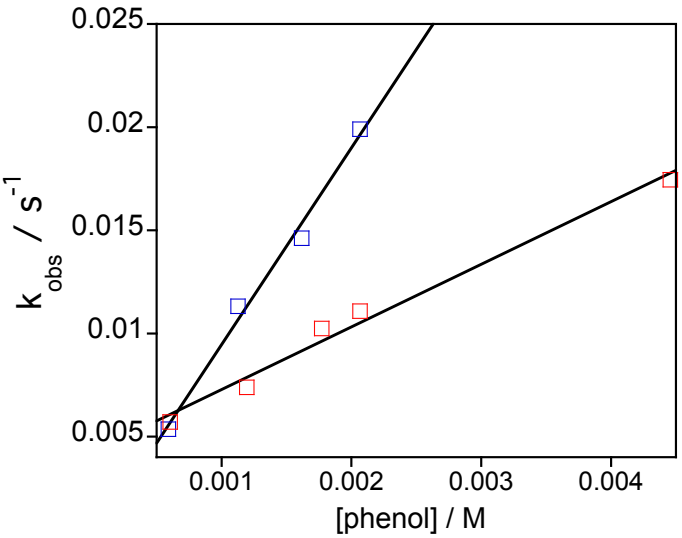

Figure S11. Second order plots of $Mn^{IV}(O)(TBP_8Cz^{\bullet+}):B(C_6F_5)_3$ with 2,4,6-TTBP (blue) and 2,4,6-TTBP-OD (red). Ratio of the second-order rate constants obtained from the slopes of the best fit lines gives a KIE (k_H/k_D) of 3.2 ± 0.3.